Journal of Cellular Physiology

Neurogenesis of Neural Crest-Derived Periodontal Ligament Stem Cells by EGF and bFGF

VERONICA R. FORTINO,[1] REN-SHIANG CHEN,[2,3] DANIEL PELAEZ,[4] AND HERMAN S. CHEUNG[1,4]*

[1]*Department of Biomedical Engineering, College of Engineering, University of Miami, Coral Gables, Florida*

[2]*Department of Physiology and Biophysics, Miller School of Medicine, University of Miami, Miami, Florida*

[3]*Department of Life Science, Tunghai University, Taichung, Taiwan*

[4]*Geriatric Research, Education and Clinical Center (GRECC), Miami Veterans Affairs Medical Center, Miami, Florida*

Neuroregenerative medicine is an ever-growing field in which regeneration of lost cells/tissues due to a neurodegenerative disease is the ultimate goal. With the scarcity of available replacement alternatives, stem cells provide an attractive source for regenerating neural tissue. While many stem cell sources exist, including: mesenchymal stem cells, embryonic stem cells, and induced pluripotent stem cells, the limited cellular potency, technical difficulties, and ethical considerations associated with these make finding alternate sources a desirable goal. Periodontal ligament stem cells (PDLSCs) derived from the neural crest were induced into neural-like cells using a combination of epidermal growth factor, and basic fibroblast growth factor. Morphological changes were evident in our treated group, seen under both light microscopy and scanning electron microscopy. A statistically significant increase in the expression of neuron-specific β-tubulin III and the neural stem/progenitor cell marker nestin, along with positive immunohistochemical staining for glial fibrillary acidic protein, demonstrated the success of our treatment in inducing both neuronal and glial phenotypes. Positive staining for synaptophysin demonstrated neural connections and electrophysiological recordings indicated that when subjected to whole-cell patch clamping, our treated cells displayed inward currents conducted through voltage-gated sodium (Na^+) channels. Taken together, our results indicate the success of our treatment in inducing PDLSCs to neural-like cells. The ease of sourcing and expansion, their embryologic neural crest origin, and the lack of ethical implications in their use make PDLSCs an attractive source for use in neuroregenerative medicine.

J. Cell. Physiol. 229: 479–488, 2014.

Neuroregenerative medicine aims to replace, regenerate, or arrest the loss of cells and tissues due to neurodegenerative and neurological disorders, in order to restore normal function. Often, however, obtaining sufficient replacement amounts of mature cells and/or tissues is difficult and technically challenging. Stem cells, derived from various tissue sources and capable of differentiating into many cell types, provide an attractive option for cellular therapies in neurological diseases. Stem cells in the body differentiate into several cell types based on various environmental cues, and studies have shown that neural-like and glial-like cells can be successfully generated from multiple (human and animal) stem cells (Kim and de Vellis, 2009), including induced pluripotent stem cells (Kuo and Chang, 2012; Kuo and Wang, 2012), embryonic stem cells (ESCs) (Ostrakhovitch et al., 2012), mesenchymal stem/stromal cells (MSCs) (Cardozo et al., 2012), and neural stem cells (Ostrakhovitch et al., 2012; Ribeiro et al., 2012). MSCs, the most widely studied stem cell type, have undergone several protocols for generating neural-like cells. Recent methods for inducing MSCs (human and animal) to neural-like cells in vitro have included: chemical moiety and growth factor induction (Cheng et al., 2009; Li and Tian, 2009; Jang et al., 2010; Qian et al., 2010), microRNA transfection techniques (Zhou et al., 2012), and growth of the cells onto different biomaterial/extracellular matrix surfaces (D'Angelo et al., 2010; Mruthyunjaya et al., 2010). Despite the lack of attaining functional neural tissues from these protocols, the concept of pre-conditioning stem cells down a given lineage is an important one in avoiding the formation of other undesired cell types when transplanted in vivo.

Author contributions: V.R.F.—conception and design of experiments, collection and assembly of data, data analysis and interpretation, manuscript writing, final approval of manuscript; R.S.C.—design of experiments, collection and assembly of data, data analysis and interpretation, manuscript writing, final approval of manuscript; D.P.—conception and design of experiments, collection and assembly of data, manuscript review and revision, final approval of manuscript; H.S.C.—conception and design of experiments, data analysis and interpretation, manuscript review and revision, final approval of manuscript, financial support, provision of study materials.

Conflict of interest: The authors state that no competing financial interests exist.

*Correspondence to: Herman S. Cheung, Miami VA Medical Center, 1201 NW 16th Street, Miami, FL 33125.
E-mail: hcheung@med.miami.edu

Manuscript Received 17 July 2013
Manuscript Accepted 6 September 2013

Accepted manuscript online in Wiley Online Library (wileyonlinelibrary.com): 16 September 2013.
DOI: 10.1002/jcp.24468

Given the rising incidence of neurodegenerative diseases in today's society, an emphasis on different cell sources which may be required for a variety of neurodegenerative diseases, as well as the need for optimization of differentiation protocols has recently been highlighted (Gögel et al., 2011). Additionally, stem cell sourcing methods and ethical implications need to be addressed in order to make stem cell therapies available to the public. For this reason, a cell type that is easily acquired during routine medical practices and devoid of the ethical dilemmas surrounding the use of other stem cell sources is preferred for neuroregenerative cellular therapies.

Our lab has recently isolated a unique pluripotent stem cell population from adult human periodontal ligament (PDL). The PDL is a soft connective tissue embedded between the tooth root and the alveolar socket. In our initial characterization of this cell type, it was found that these PDL stem cells (PDLSCs) expressed both ESC and neural crest cell specific surface markers (i.e., SSEA-3, SSEA-4, TRA-1-60). They also exhibited gene expressions of Oct4, Nanog, Sox2, and Klf4 (Huang et al., 2009) genes which have been successfully used to reprogram human dermal fibroblasts into pluripotent ESC-like cells.

Not surprisingly, due to the location of the periodontal ligament, most of the research into differentiation of PDLSCs has been geared towards osteogenic lineages (Chen et al., 2012; Lee et al., 2012; Singhatanadgit and Varodomrujiranon, 2012; Song et al., 2012; Wu et al., 2012; Zhang et al., 2012a). Interestingly, however, it is now widely accepted that the periodontal ligament is a derivative of the neural crest in vertebrates (Coura et al., 2008; Dupin and Sommer, 2012) and is also considered a niche for post-migratory neural crest-derived multipotent cells (Dupin and Coelho-Aguiar, 2012).

Several cell types are derived from the migrating neural crest, including most of the cells of the peripheral nervous system: sensory, sympathetic, parasympathetic and enteric ganglia, sensory neurons and glia of the dorsal root ganglia, cephalic ganglia, satellite glial cells of all autonomic and sensory ganglia, and Schwann cells of all the peripheral nerves (Le Douarin and Kalcheim, 1999). As both PDLSCs and many mature neural types are derived from the same embryologic neural crest, stem cells of the periodontal ligament are less lineage-divergent to neural cells than other types of stem cells.

Our approach, therefore, was to characterize and induce PDLSCs based on their embryological origin and treat them as neural crest cells. In a study by Garcez et al., quail trunk neural crest cells were exposed to a epidermal growth factor (EGF) and basic fibroblast growth factor (bFGF) cocktail, demonstrating for the first time that EGF induced differentiation of neural crest cells to a neuronal phenotype while bFGF induced a glial phenotype (Garcez et al., 2009). The objective of this study was to determine if neural-like cells could be generated from our population of neural crest-derived periodontal ligament stem cells (PDLSCs). Our methods, therefore, are unique in that we characterize and neuro-induce our cells as neural crest cells instead of purely mesenchymal cells.

The question our research sought to answer was whether or not stem cells taken from the periodontal ligament could be induced into neural-like cells using a simple and short method, thus making it easy for other neuroregenerative medicine researchers to obtain neural-like cells from PDLSC. Our neuro-induction treatment consisted of adding EGF and bFGF to complete culture media and grow the PDLSCs in vitro for 8 days. Following our neuro-induction treatment, we were able to see morphologic, genotypic, phenotypic, and electrophysiological changes indicative of a neural-like cell, indicating that our neuro-induction treatment was effective at driving PDLSCs to neural-like cells.

Materials and Methods

Culture media and other reagents

High glucose complete culture medium (HGCCM)—high glucose Dulbecco's modified eagle medium supplemented with 10% fetal bovine serum (FBS), 1% penicillin streptomycin (100 U/ml penicillin and 100 μg/ml streptomycin), and 0.1% amphotericin B (0.25 μg/ml).

Culturing of PDLSCs

PDLSCs were harvested from impacted wisdom teeth following our IRB approved protocols as previously described (Huang et al., 2009). Briefly, the periodontal ligaments from the same donor (following wisdom teeth removal) were finely chopped and placed in an epi tube with digestion media overnight in 37°C. Single cell suspensions were obtained by passing the resulting digestion through a 70 μm cell strainer. Cells were placed in culture dishes for 5 days and all non-adherent cells were removed by changing the media on the 5th day. Once the cells reached ~70% confluency they were lifted and plated in T75 culture flasks with HGCCM for further expansion (P1), and passaged again when they reached ~70% confluence. Cells that were passage 4 from a single cell line were used for all experiments as they were readily available in the lab; PDLSCs maintain their stem-like properties and proliferate at the same rate at both lower and higher passages. PDLSCs were separated into two groups: control and EGF + bFGF treated. This treatment was modified from a previous paper by Delcroix et al. (2010), where 50 ng/ml of EGF and bFGF were found to be the optimal concentrations of these growth factors. All cells were plated at a density of 4,000 cells/well in 6-well tissue culture plastic plates. All cells were plated using HGCCM. Cells were allowed to adhere to the plates overnight. Media was removed the following day and treatments were begun. The control cells were cultured in HGCCM for the duration of the experiment. EGF and bFGF were added to the EGF + bFGF treated group at a concentration of 50 ng/ml. Media was changed every 2 days for a total of 8 days of treatment. Cells were then collected for RNA extraction or fixed for immunohistochemical staining.

RNA extraction, cDNA synthesis, and qPCR

At the end of the treatment, cells used for gene expression analysis were collected and Trizol extraction was performed (Invitrogen, part of Life Technologies, Grand Island, NY) per the manufacturer's instructions with the following modifications: centrifugation for phase separation and RNA precipitation was done at 14,000 rpm for 20 min. Centrifugation for the RNA wash was done at 7,500 rpm for 10 min. Total RNA yield was determined using the NanoDrop ND-1000 spectrophotometer (Thermo Scientific, Wilmington, DE). Total RNA (1 μg) was converted to cDNA using the ABI High Capacity cDNA Reverse Transcription Kit (Applied Biosystems, part of Life Technologies, Grand Island, NY) and the GeneAmp PCR System 9700 (Applied Biosystems). Quantitative PCR (qPCR) was performed using the Stratagene Mx3005P (Agilent Technologies, Santa Clara, CA). The samples were prepared using the Sybr Green PCR master mix (Applied Biosystems), with 20 ng cDNA per reaction. The genes evaluated along with their primer sequences are in Table I. Primer sequences were designed based on the corresponding human genes.

Scanning electron microscopy (SEM)

Tissue culture coverslips (13 mm round) were coated for 5 min with 0.1% gelatin filtered through a 0.8 μm filter. After 5 min the gelatin was removed and the culture rounds were washed once with phosphate buffered saline (PBS). PDLSCs were seeded unto the culture rounds at a density of 2,500 cells/tissue culture round.

TABLE I. Genes for qPCR*

Gene	Accession number	Forward primer 5′–3′	Reverse primer 5′–3′
CD133	NM_006017.1	GATGCCTCTGGTGGGGTATTTC	TTTCCTTCTGTCGCTGGTGC
SOX1	NM_005986	TGCTGGATTCTCACACAC	CTCGTCAGGAATAATGAACAAG
Nestin	NM_006617.1	ATCAGATGACATTAAGAC	CTTCAGTGATTCTAGGAT
Noggin (NOG)	NM_005450	AACTGTGTAGGAATGTATATGTG	ATTAGCAACAACCAGAATAAGT
β-tubulin III (TUBB3)	NM_006086	CAAGTTCTGGGAAGTCATCA	TTGTAGTAGACGCTGATCC
Neurofilament medium (NEFM)	NG_008388	TTGGCAAGGGAAACAAACAC	TCAGGGAAATTGGGATGTATATGT

*The genes and PubMed accession numbers for the specific genes tested using qPCR. The forward and reverse primers for each gene are shown.

All cells were plated using HGCCM. Cells were allowed to adhere to the tissue culture rounds overnight. Media was removed the following day and treatments were begun. The control cells were cultured in HGCCM for the duration of the experiment. EGF and bFGF were added to the EGF + bFGF treated group at a concentration of 50 ng/ml. Media was changed every 2 days for a total of 8 days of treatment. After completing the treatment, the media was removed and samples were fixed with Millonigs phosphate buffer + 2.5% glutaraldehyde. Samples were kept at 4°C until further processing. Once ready for processing the samples were rinsed three times for 5 min with the Millonigs phosphate buffer. Half strength Millonigs phosphate buffer was added to the samples with 1% OsO_4 and left to incubate at room temperature for 1.5 h. Following incubation the Millonigs and OsO_4 were removed and the samples were once again rinsed three times for 5 min with Millonigs phosphate buffer. A dehydration series was performed with 50%, 70%, and 95% acetone where the acetone was added and incubated for 5 min, removed, and the same concentration was once again added and left for 10 min. Following the removal of the 95% acetone, 100% acetone was added to each sample and incubated for 10 min. The acetone was removed and addition of 100% acetone was repeated three more times for a total of four incubations with 100% acetone. The 100% acetone was decanted and critical point drying was performed using Hexamethyldisilazane (HMDS). A 2:1, 1:1, and 1:2 ratio of acetone to HMDS was added to the samples with wait times of 10 min in between removal and addition of HMDS. The 1:2 ratio of acetone: HMDS was removed and 100% HMDS was added to each sample. The samples were incubated for 5 min and the HMDS was removed. This was done one more time with 100% HMDS. The samples were removed from the HMDS and allowed to dry. The samples were then mounted onto 1 cm SEM sample stubs and sputter coated using a Hummer 6.2 sputter coater per the manufacturer's instructions. Samples were then imaged using a Jeol 5600 LV Scanning Electron Microscope at 10 kV. Adobe Photoshop or Microsoft Publisher was used for image processing.

Immunohistochemistry

Following treatment and culture, cells used for immunohistochemistry were washed once with PBS. PBS was removed and cells were fixed with either 10% formalin (cell membrane markers) or 100% ice-cold methanol (intracellular markers) for 10 min. After removal of the fixative the cells were washed twice with PBS and remained in PBS at 4°C until processed. Cell membrane marker samples were blocked for 1 h in 5 mg/mL bovine serum albumin (BSA) in PBS. Intracellular marker samples were blocked for 1 h in PBS + 0.05% Tween 20 + 2% BSA + 1% FBS. Immunostaining was carried out using the following primary antibodies and dilutions in 0.5 mg/ml BSA in PBS: synaptophysin—1:150 (Millipore, Billerica, MA), neuron-specific beta-tubulin III—1:100 (Abcam, Cambridge, MA), glial fibrillary acidic protein (GFAP)—1:1,000 (Abcam, Cambridge, MA). Cells were left incubating in the primary antibodies overnight. The following day, the primary antibody was discarded and the cells were washed twice in PBS. The following secondary antibodies were applied diluted 1:200 in PBS: synaptophysin, goat pAb to Ms IgG (FITC); β-tubulin III, bovine anti mouse IgG (Rhodamine); GFAP, goat pAb to Rb IgG (FITC) (all secondary antibodies: Abcam). The samples were shielded from light and incubated for 2 h. For the synaptophysin staining, the secondary antibody was discarded following the 2-h incubation and the samples were washed once with PBS. An Alexa Fluor 568 Phalloidin (Life Technologies, Grand Island, NY) was added to PBS at a 1:25 dilution and placed in the sample well. The sample was shielded from light and left to incubate for 30 min. Following the 30 min incubation, the Alexa Fluor was removed and the wells were washed once with PBS. For all samples, two drops of Vectashield hard set mounting media with DAPI (Fischer Scientific, Hampton, NH) was placed in each well. A glass coverslip was thoroughly washed, dried, and placed in each well. The samples were shielded from light and taken to image. Immunohistochemical images were acquired using a Nikon Digital Camera DS-Qi1MC mounted to a Nikon Eclipse Ti inverted fluorescent microscope. The NIS Elements software package was used for merging images and image analysis.

Electrophysiology

Dishes (35 mm^2) were plated with PDLSCs at a density of 50 cells/dish. All cells were plated using HGCCM. Cells were allowed to adhere to the dishes overnight. Media was removed the following day and replaced with fresh HGCCM in order to allow the cells to proliferate to the desired confluency. Following an additional 2 days, the media was removed and the treatments were begun. EGF and bFGF were added to the EGF + bFGF treated group at a concentration of 50 ng/ml. Media was changed every 2 days for a total of 8 days of treatment. After completing the treatment, inward and outward currents were recorded in the whole-cell voltage-clamp configuration with an Axopatch 200A amplifier, Digidata 1322A interface, and pClamp 9.0 software (Molecular Devices, Sunnyvale, CA). Data were sampled at 50 kHz and low-pass filtered at 5 kHz before off-line filtered at 2 kHz for final analysis. Borosilicate pipettes with 2–5 megaohm resistance were used when placed in the bath solution. The pipette solution contained (in mM): 130 K-gluconate, 10 KCl, 1 $MgCl_2$, 1 $CaCl_2$, 1 EGTA, and 10 HEPES, pH 7.2. The bath solution contained (in mM): 140 NaCl, 5 KCl, 2 $MgCl_2$, 2 $CaCl_2$, 10 glucose, and 10 HEPES, pH 7.4. For sodium-free experiments the K-gluconate and KCl in the pipette solution were replaced by 140 mM CsCl, and the NaCl in the bath solution was replaced by 140 mM N-methyl-D-glucamine chloride. Leaks and capacitive transients were online subtracted using the p/-4 or p/-5 leak subtraction routine.

Statistical analysis

Gene expression. Values from three independent experiments were pooled for the analysis. Data were analyzed using the Delta-Delta-CT Method, with the samples being normalized both to control samples and to the housekeeping gene GAPDH. Resulting data were analyzed with a 2-tailed Student's *t*-

test, with $P < 0.05$ considered significant. The resulting values were reported and plotted as mean ± SEM. Electrophysiology: 2-tailed Student's *t*-test assuming equal variances was used to analyze the peak inward currents between control and treated groups at voltages indicated in the figure. Data were reported and plotted as mean ± SEM.

Results

Gene expression

Following treatment with EGF + bFGF, several genetic marker categories were examined with qPCR to determine changes cell genotype: adult/neural stem cell (CD133, SOX1, noggin [NOG]), neural progenitor/immature neuron (β-III tubulin [TUBB3] and nestin), and mature neuron (neurofilament medium, NEFM). Genetic analysis demonstrated significant changes in the gene expression of several key genes following treatment with EGF + bFGF (Fig. 1). In particular, there was a statistically significant increase in the expression of the neural progenitor/immature neuron markers nestin ($P < 0.0001$) and TUBB3 ($P < 0.01$). SOX1, one of the neural stem cell genes showed a marked increase in expression, along with NEFM, a mature neuron marker. Interestingly, the expression of NOG significantly decreased ($P < 0.0001$) following our induction protocol. Taken together, the results from the gene expression suggest that our induction protocol is taking the PDLSC from a multipotent state to a neural lineage.

Scanning electron microscopy

Morphological differences between the EGF + bFGF treated cells versus control cells were apparent under a light microscope (Fig. 2). As expected, cells undergoing differentiation did not proliferate as much as the control cells, making the control cells more confluent at the end of the 8 day treatment as opposed to the neural-induced PDLSCs. Both control (Fig. 2A and B) and treated PDLSCs (Fig. 2C and D) are shown with the differences clearly visible. The control PDLSCs coalesce and form no visible cell–cell connections (Fig. 2A). Once the control cells at a higher magnification are observed, the cell bodies are wide and the cells do not have any visible neurites (Fig. 2B). This is very different than the treated PDLSCs, which begin to connect and form networks (Fig. 2C) and have neurites extending from the rounded and raised cell bodies (Fig. 2D).

To explore this morphological difference in depth, SEM was used to analyze morphological differences at both low and high magnifications following the 8 days of EGF + bFGF treatment. Under the scanning electron microscope the differences between the control and treated cells were easily and strongly visible. The control cells (Fig. 3A) formed what appears to be a sheet of cells in contrast to the EGF + bFGF treated cells, which formed a network (Fig. 4A). Even through increasing the magnification, the individual control cells were still not visible (Fig. 3B–F) and further demonstrated a coalescing sheet instead of network. In contrast, the EGF + bFGF treated PDLSCs (Fig. 4) strongly presented morphologies typical of neural-like cells. A network is clearly seen at low magnifications (Fig. 4A) and also at high magnifications (Fig. 4C), when the neural-like cell can be distinctly seen making connections with neighboring cells. Both neural-like and glial phenotypes were identified in the in vitro culture of EGF + bFGF treated PDLSCs (Fig. 4B, D, and E). The neural-like cells are clearly distinguished by their rounded and raised cell bodies and very thin neurite-like processes that branch further and connect to nearby cells (Fig. 4A, B, C, and E). Glial-like cells appear flatter and wider,

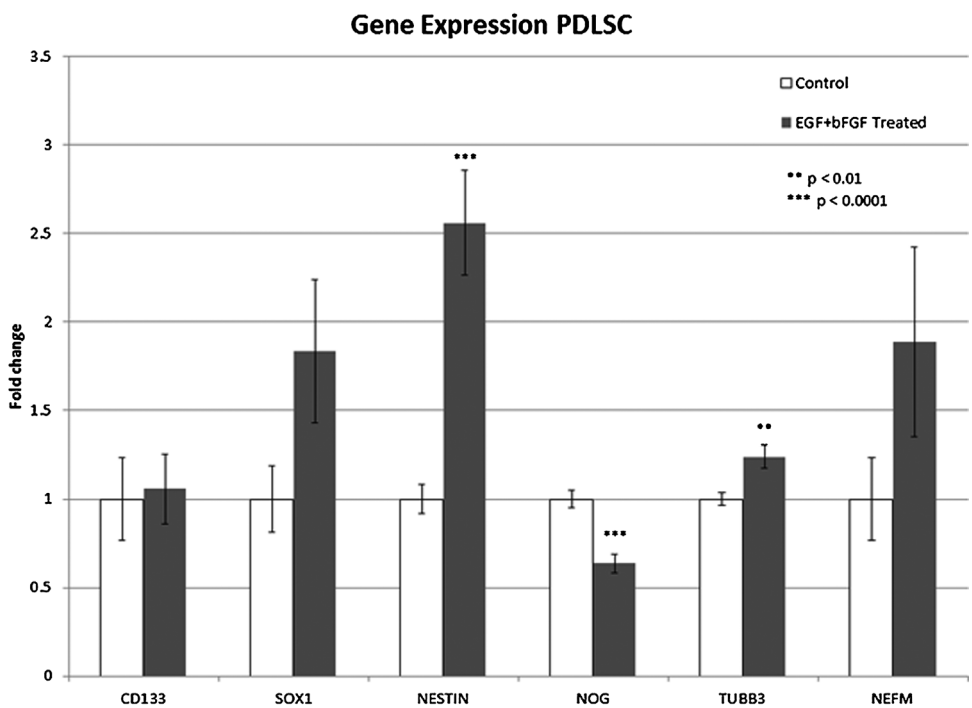

Fig. 1. Gene expression of PDLSCs following EGF + bFGF Treatment. A significant increase can be seen in key immature neuron/progenitor markers following EGF + bFGF treatment (TUBB3 $P < 0.01$, NESTIN $P < 0.0001$). A significant decrease is also seen in NOG ($P < 0.0001$). Data was pooled from 3 separate experiments. control n = 12, treated n = 18. Data reported as mean ± SEM.

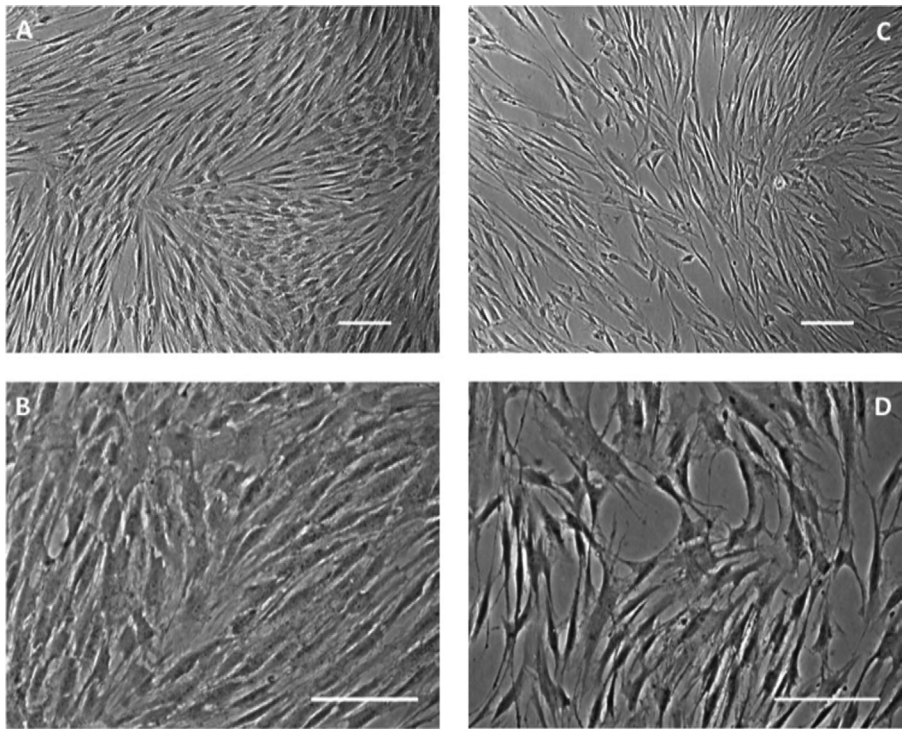

Fig. 2. PDLSCs under light microscope. (A, B) Control PDLSCs. (A) Control PDLSCs coalesce and form no visible cell–cell connections. Scale bar = 100μm. (B) Under higher magnification, the cell bodies of the control PDLSCs are wide and the cells do not have any visible neurites. Scale bar = 100μm. (C, D) EGF + bFGF treated PDLSCs. (C) Treated PDLSCs connect and begin to form networks. Scale bar = 100μm. (D) At a higher magnification, it is clearly seen that the cell bodies of the treated PDLSCs are rounder and higher than the control cells with visible neurites. Scale bar = 100μm.

with thicker processes that extend to neighboring cells (Fig. 4B and D). As stated previously, the control cells looked very different and presented no morphological similarities to neural-like cells (Fig. 3). These images suggest that our neuro-induction protocol is effective at producing morphologically correct phenotypes of both glial and neuronal progenitor cells.

Immunohistochemical staining

While the SEM images demonstrated morphological presentation of both glial and neuronal-like cells, further verification of the success of our treatment was assessed by immunohistochemical analysis. Immunohistochemical analysis of neurogenic-induced cells shows positive staining for both neuron-specific β-tubulin III (TUBB3) and the astrocyte-specific marker glial fibrillary acidic protein (GFAP) (Fig. 5). Corroborating observations made under SEM, the cells that presented a compact, raised, and rounded cytoplasm with neurite-like processes were positive for TUBB3 (Fig. 5B) while the cells that had a flatter cytoplasm and broader process stained positive for GFAP (Fig. 5A). The proteins were correctly presented and suggest that our induction protocol is successful at producing neural-like cells, both glial and neuronal phenotypes. The control cells, however, demonstrated no visible staining for either of these proteins (images not shown). Synaptophysin, a synaptic vesicle glycoprotein commonly located at pre-synaptic terminals, was also present in the EGF + bFGF treated group (Fig. 5C). Synaptophysin staining was not present in the control group (images not shown). These findings further demonstrate that our neuro-induction protocol is effective at producing neural-like cells that present a correct neural phenotype. Additionally, both neural cell types are present, indicating that our neuro-induction protocol is effective at inducing both glial and neuronal populations.

Electrophysiology

In order to assess whether synatophysin presentation correlated to functional electrophysiological properties in neurogenic-induced PDLSCs, patch clamping was performed. Although preliminary current-clamping experiments on EGF + bFGF treated PDLSCs failed to elicit action potentials, voltage-clamp experiments demonstrated active ionic currents in EGF + bFGF treated PDLSCs. These cells contained both fast-inactivating inward and slow-outward currents during voltage jumps to various voltages from a holding voltage of −100 mV (Fig. 6A); fast-inactivating inward currents and slow but sustained outward currents are shown in 20 mV steps. The fast-inactivating currents peaked around −10 mV, having kinetics and a range of activation similar to voltage-activated sodium currents. When peak outward and inward current densities, measured as current amplitude per unit cell capacitance (proportion to cell surface area), were plotted against testing pulse voltages, they looked similar to the fast Na^+ current and delayed-rectifier K^+ currents in neurons (Fig. 6B). Interestingly, after treatment with EGF + bFGF, the neural-like PDLSC cells exhibited increased Na^+-like current density, while the outward K^+ current density stayed the same. To test if the increased inward currents were indeed Na^+ currents, the Na^+ in the external bath was replaced with NMDG; it was found that no inward currents were observable while the recorded outward currents slightly increased over

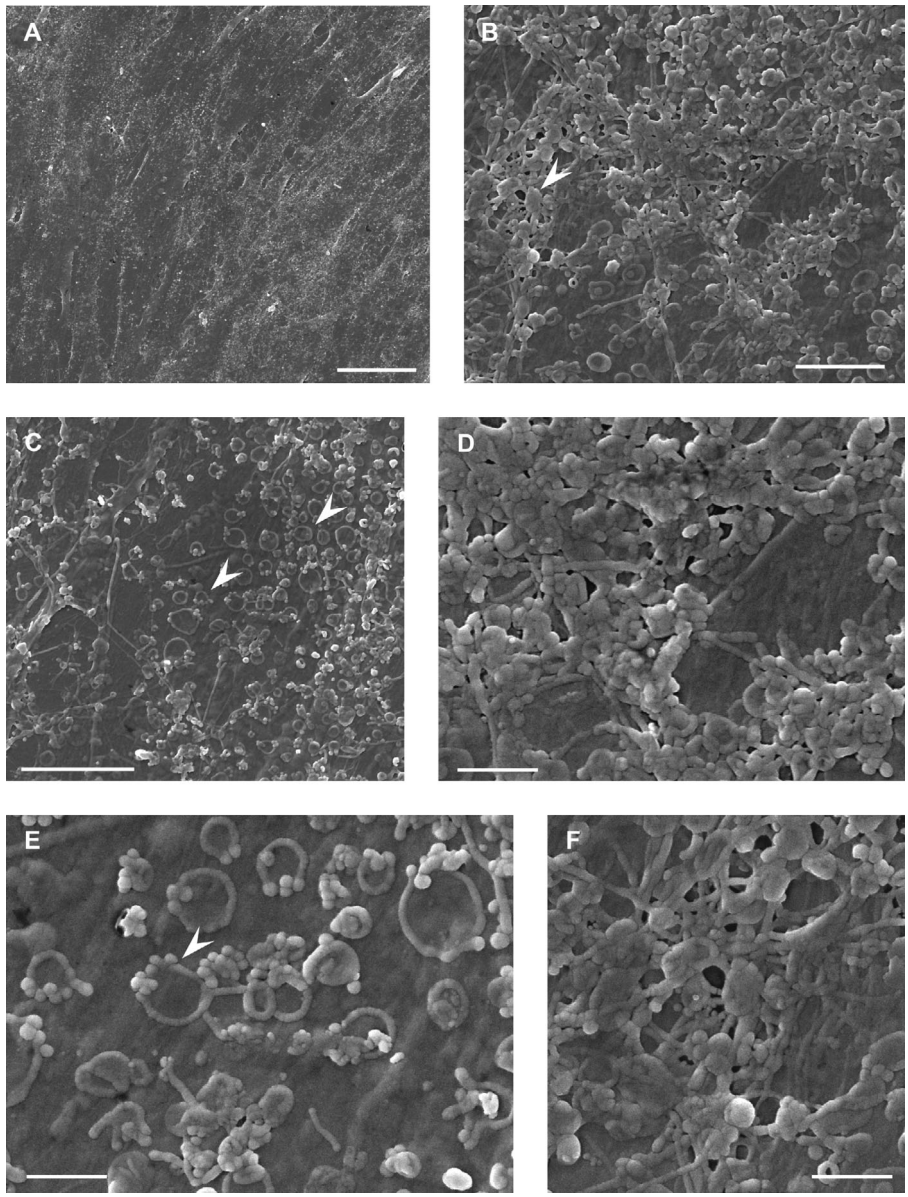

Fig. 3. SEM of Untreated PDLSCs. (A) Surface view of the confluent layer of control cells. Scale bar = 50μm. The control PDLSCs coalesce into a sheet rather than forming a network of cells, and exhibit no neural morphologies. (B) Increased magnification of surface of cells – processes connecting one cell to another and protein globules can be seen (white arrowhead). Scale bar = 5μm. (C) View of endocytotic/ endocytic vesicles on the cell membrane (white arrowhead). Scale bar = 10μm. (E) Magnified view of (C). The vesicles are seen grouped together with what appears to be mini vesicles on their periphery (white arrowhead). Scale bar = 2μm. (D), (F) Magnified view of (B). Scale bar = 2μm.

the range where Na^+-like currents were activated. Significant differences ($P < 0.01$, *t*-test) were found for the inward currents between control and neural-like PDLSCs at the four voltages tested (Fig. 6B). Sodium channels are the basis for an action potential in neurons. This indicates, therefore, that the inward current that responds to the EGF + bFGF treatment is indeed from voltage-gated Na^+ channels, and that the EGF + bFGF treatment is successful in eliciting these responses from our treated PDLSC. A standard two-pulse protocol (Fig. 6C) was used to characterize voltage-dependent inactivation (a characteristic of voltage-gated Na^+ channels) of the inward currents in neural-like PDLSCs. In the two-pulse protocol, the current availability during the test pulse was used to evaluate the amount of inactivation during the first pulse or prepulse. Inward currents were induced similarly as in (A), but stepped briefly (1.5 msec) to −100 mV before tested again at +10 mV. As can be seen in Figure 6C, the more channels activated during the prepulses, the fewer channels that remained available for opening during the second testing pulse at +10 mV. Typical voltage-dependent inactivation for Na^+ channels was found (Fig. 6D). Voltage-dependent inactivation of the inward currents were normalized to the maximal and minimal currents in each cell before being averaged and fitted with the Boltzmann equation: $I/I_{max} = 1/$

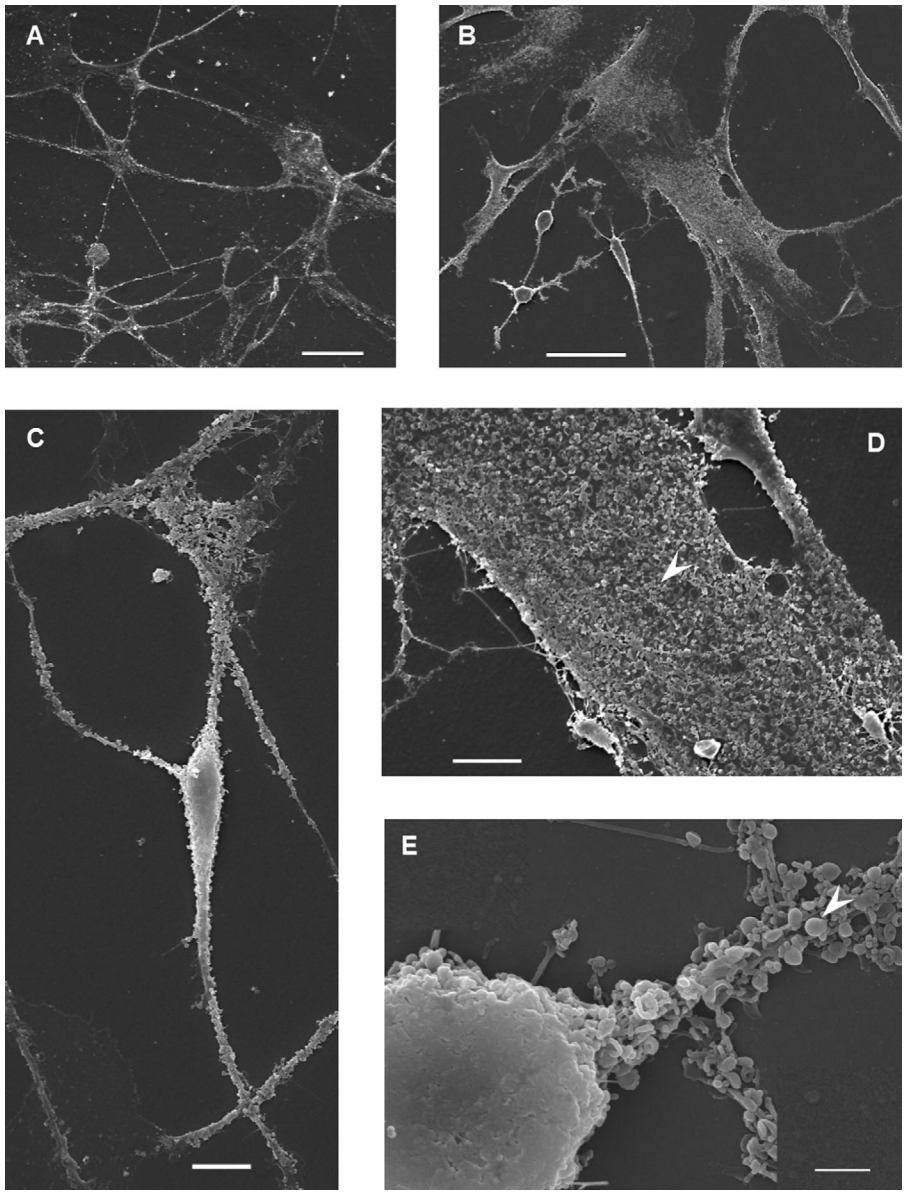

Fig. 4. SEM of EGF + bFGF treated PDLSCs. (A) Surface view of the layer of treated cells forming a neural network. Scale bar = 50μm. (B) Treated PDLSCs demonstrate two distinct phenotypes. The glial phenotype is seen as being wide and flat, with thick processes. The neuronal phenotype is seen as a more rounded and raised cell body, with thin processes that then have further branching. Scale bar = 50μm. (C) The treatment induces a neuronal phenotype with a raised cell body, with thin processes. The processes are seen to connect to processes from other cells. Scale bar = 10μm. (D), (E) Magnified view of (B). (D) Surface of the glial cell. Numerous endocytotic/endocytic vesicles can be seen along with globular proteins on the cell surface (white arrowhead). Scale bar = 10μm. (E) Cell body of the neuron along with its extended process. The thin fibril-like cytoskeleton can be seen covered with globular proteins (white arrowhead). Scale bar = 2μm.

$\{1 + \exp[(V + 40.0\,\text{mV})/13.55\,\text{mV}]\}$; this resulted in a half-inactivation voltage at −40 mV.

Discussion

The aforementioned experiments, taken together, support the hypothesis that a neuro-induction treatment consisting of EGF and bFGF induces a neural-like cell from PDLSCs. The presented induction protocol is successful at generating both neural phenotypes: glial (Fig. 4B, upper right, 4D) and neuronal-like cells (Fig. 4A, B lower right, C, and E).

The gene expression data (Fig. 1) suggested that the PDLSCs are moving towards a neural genotype and demonstrate some very interesting genetic changes. Firstly, the human stem cell marker CD133 did not see any statistically significant changes following the EGF + bFGF neuro-induction treatment. We believe that this is because as not 100% of the cells differentiated into neural cells some of them remained in the multipotent stem cell state. Interestingly, both SOX1 (a neural stem cell marker) and NEFM (a mature neuronal marker) markedly increased, although not statistically significant. We believe that this is due to the stem cells differentiating at different rates; some of the PDLSCs were becoming neural

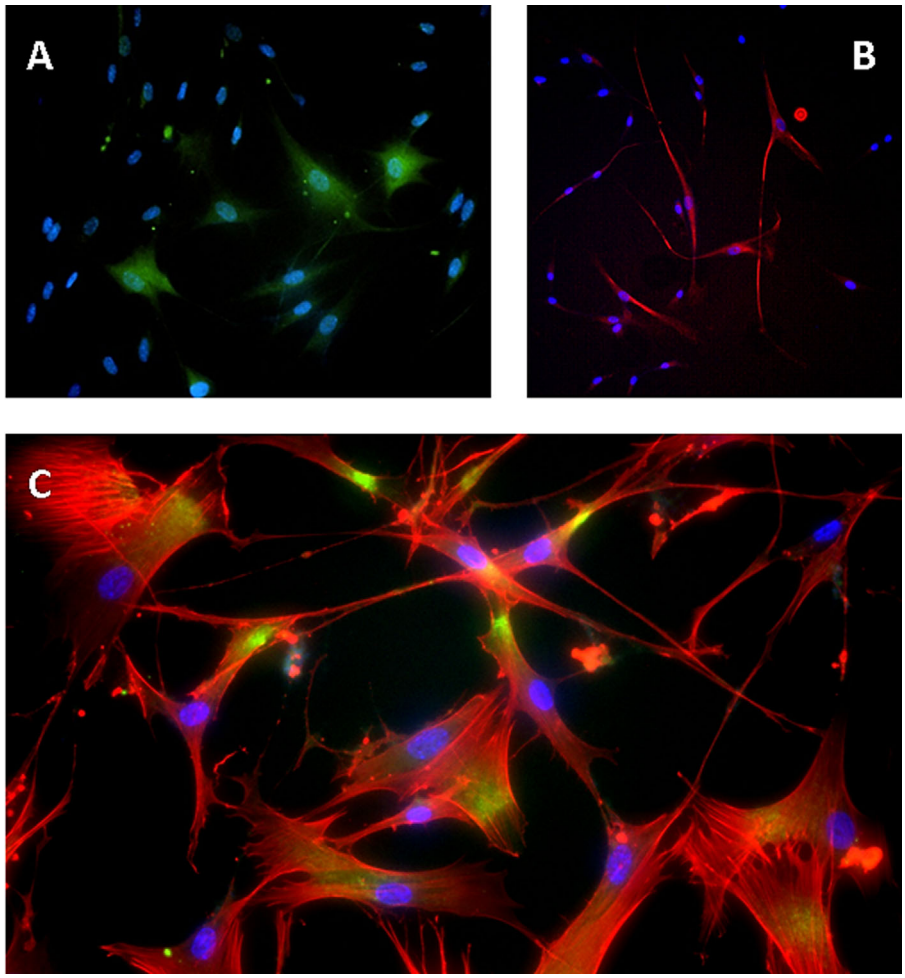

Fig. 5. Immunohistochemical Staining for EGF + bFGF treated PDLSCs. (A) GFAP for EGF + bFGF treated PDLSCs. GFAP is green and DAPI is blue. (B) TUBB3 for EGF + bFGF treated PDLSCs. TUBB3 is red and DAPI is blue. (C) Synaptophysin for EGF + bFGF treated PDLSCs. Synaptophysin, (green/yellow), is seen where cell–cell contact occurs. Alexa Flour 568 Phalloidin (cytoskeleton stain) is red and DAPI is blue.

cells while others were well on their way to full maturity. This is confirmed in the immunohistochemical staining (Fig. 5), where we see β-tubulin III (an immature neuron marker) in some of the treated PDSLCs and synaptophysin (signifying that some cells are forming functional connections with each other), suggestive of a more mature neuronal cell type. The two genetic markers that increased significantly were nestin (NES) and β-tubulin III (TUBB3)—two immature neural markers. For this reason we feel confident in our conclusion that our neural induction treatment drives the PDLSCs to become neural progenitors. One interesting genetic change that we observed was in noggin (NOG), where it decreased significantly. The function of noggin is commonly for neuronal development—we feel that this decrease in noggin was most likely displayed by the cells that had an increase in NEFM as they were driven towards a more mature neuronal genotype.

Although other investigators have isolated MSCs from the periodontal ligament (Seo et al., 2004), and typically these cells are treated as purely mesenchymal cells (Akiyama et al., 2012), the widespread acceptance that PDLSC are neural crest-derived stem cells guides the initiative to treat them as neural crest cells. This modification opens different avenues of manipulation and differentiation to something similar to what is found in vivo for neural crest cells, potentially providing for better differentiation and manipulation protocols.

PDLSCs are a viable source of stem cells for regenerative medicine as they are easily obtainable, expandable, and, as they are derived from the neural crest, have the potential to be differentiated into many different cell types. The PDLSCs have a doubling rate of ~22 h, making them a very attractive cell source for neuroregenerative medicine. Millions of PDLSCs can be obtained from a single expansion and induced into neural-like cells. Although there is a study that demonstrates the decrease of regenerative capacity and pluripotency of periodontal ligament stem cells with age (Zhang et al., 2012b), the study has only been done on the adipocytic and osteogenic potential of these cells. This study, however, is not a factor in our findings, as low passage cells (P4) were used for all of our experiments, and all of our cell lines are from donors ages 19–22. Additionally, exciting new research has demonstrated that neural crest-derived human PDLSC engraft and differentiate into the adult mouse brain (Bueno et al., 2012). This provides an even stronger argument for the use of these cells in cellular therapy for neurodegenerative diseases.

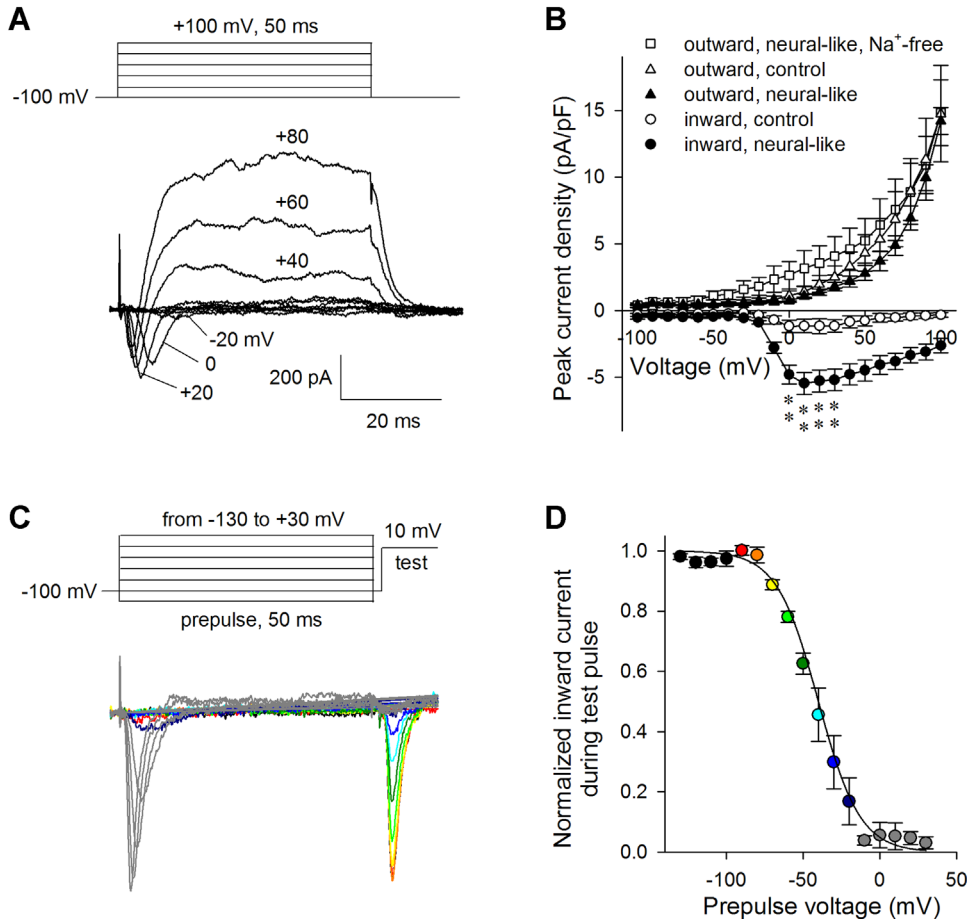

Fig. 6. Inward and outward currents of PDLSCs. (A) Representative outward and inward currents from EGF + bFGF treated PDLSCs. (B) Peak outward and inward current densities from EGF + bFGF treated PDLSCs and control PDLSCs. Mean ± SEM, N = 6. $^{**}P < 0.01$. (C) Two-pulse protocol inactivation of inward currents in EGF + bFGF treated PDLSCs, coded as in (D). (D) Voltage-dependent inactivation of inward currents in EGF + bFGF treated PDLSCs. N = 4.

This study, like any other research project, is subject to limitations. Variations in the data collected can be seen because of the heterogeneous population of PDLSCs that were used in the presented experiments. This is not a major factor, however, as the entirety of the periodontal ligament is derived from the neural crest. Similarly, despite not achieving fully functioning neurons, the explored neuro-induction protocol was capable of guiding PDLSCs towards a neural progenitor lineage.

Ongoing work is being performed to optimize neuro-induction protocols. Our lab has also recently identified and published a purified, homogeneous, pluripotent population that is comprised exclusively of neural crest-derived cells (Pelaez et al., 2013). In further studies, it will be determined whether or not the cells revert back to their stem cell state or maintain the neural phenotype in vitro once the neuro-induction treatment is completed. Additionally, studies are underway to determine the efficiency of our neuro-induction protocol to determine the amount of neurons versus glia that are obtained following induction. The ultimate goal is to produce neural cells that can be transplanted and both provide trophic support and engraft into the surrounding tissue, without reverting back to an undifferentiated state.

The present study focused on using readily available growth factors to induce PDLSCs into neural-like cells. Compared to the previously stated study (Delcroix et al., 2010), PDLSCs were successfully driven to a neural-like cell type in half the time (16–8 days). This was demonstrated using several techniques. An increase in the expression of neural markers was demonstrated with qPCR (Fig. 1). SEM visually confirmed the presence of both glial (Fig. 4B, upper right, and D) and neuronal phenotypes (Fig. 4B, lower left, A, C, and E). Immunohistochemistry later corroborated what was viewed under SEM—positive staining for both GFAP (a glial marker—Fig. 5A) and β-III tubulin (a neuronal marker—Fig. 5B). In addition to this, through positive immunohistochemical staining with synaptophysin (Fig. 5C), it was observed that the neural-like cells were forming synaptic connections with each other. Electrophysiological recordings verified the presence of inward and outward currents significantly different than the control cells (Fig. 6B) that were conducted through voltage-gated sodium (Na^+) channels (Fig. 6C). Taken together, our data suggest that our current neuro-induction protocol is successful at driving the neural crest-derived PDLSC to a more neural-like cell type. The results of this work are encouraging for neuroregenerative medicine and translational studies

because a simple and fast approach is a much needed push towards transitioning regenerative medicine from bench to bedside.

Acknowledgment

Many thanks to Yucan Zhao, who provided wonderful technical work for the gene expression portion of this manuscript. Many thanks to the Dauer Electron Microscopy Laboratory at the University of Miami for allowing us to use the facility for the SEM portion of this manuscript.

Literature Cited

Akiyama K, Chen C, Gronthos S, Shi S. 2012. Lineage differentiation of mesenchymal stem cells from dental pulp, apical papilla, and periodontal ligament. Methods Mol Biol 887:111–121.

Bueno C, Ramirez C, Rodríguez-Lozano FJ, Tabarés-Seisdedos R, Rodenas M, Moraleda JM, Jones JR, Martinez S. 2012. Human adult periodontal ligament-derived cells integrate and differentiate after implantation into the adult mammalian brain. Cell Transplant Oct 3. Epub ahead of print.

Cardozo AJ, Gómez DE, Argibay PF. 2012. Neurogenic differentiation of human adipose-derived stem cells: Relevance of different signaling molecules, transcription factors, and key marker genes. Gene S0378-1119:01119-5.

Chen CY, Liu YJ, Shi SG, Chen FM, Cai C, Li B, Wang J, Shi L, Li Y, Liu ZY, Niu ZY. 2012. Osteogenic differentiation of human periodontal ligament stem cells expressing lentiviral NEL-like protein 1. Int J Mol Med 30:863–869.

Cheng Z, Zheng Q, Wang W, Guo X, Wu Y, Zheng J. 2009. Targeted induction of differentiation of human bone mesenchymal stem cells into neuron-like cells. J Huazhong Univ Sci Technolog Med Sci 29:296–299.

Coura GS, Garcez RC, de Aguiar CB, Alvarez-Silva M, Magini RS, Trentin AG. 2008. Human periodontal ligament: A niche of neural crest stem cells. J Periodontal Res 43:531–536.

D'Angelo F, Armentano I, Mattioli S, Crispoltoni L, Tiribuzi R, Cerulli GG, Palmerini CA, Kenny JM, Martino S, Orlacchio A. 2010. Micropatterned hydrogenated amorphous carbon guides mesenchymal stem cells towards neuronal differentiation. Eur Cell Mater 20:231–244.

Delcroix GJ, Curtis KM, Schiller PC, Montero-Menei CN. 2010. EGF and bFGF pre-treatment enhances neural specification and the response to neuronal commitment of MIAMI cells. Differentiation 80:213–227.

Dupin E, Coelho-Aguiar JM. 2012. Isolation and differentiation properties of neural crest stem cells. Cytometry A 83:38–47.

Dupin E, Sommer L. 2012. Neural crest progenitors and stem cells: From early development to adulthood. Dev Biol 366:83–95.

Garcez RC, Teixeira BL, Schmitt Sdos S, Alvarez-Silva M, Trentin AG. 2009. Epidermal growth factor (EGF) promotes the in vitro differentiation of neural crest cells to neurons and melanocytes. Cell Mol Neurobiol 29:1087–1091.

Gögel S, Gubernator M, Minger SL. 2011. Progress and prospects: Stem cells and neurological diseases. Gene Ther 18:1–6.

Huang CY, Pelaez D, Dominguez-Bendala J, Garcia-Godoy F, Cheung HS. 2009. Plasticity of stem cells derived from adult periodontal ligament. Regen Med 4:809–821.

Jang S, Cho HH, Cho YB, Park JS, Jeong HS. 2010. Functional neural differentiation of human adipose tissue-derived stem cells using bFGF and forskolin. BMC Cell Biol 11:25.

Kim SU, de Vellis J. 2009. Stem cell-based cell therapy in neurological diseases: A review. J Neurosci Res 87:2183–2200.

Kuo YC, Chang YH. 2012. Differentiation of induced pluripotent stem cells toward neurons in hydrogel biomaterials. Colloids Surf B Biointerfaces 102C:405–411.

Kuo YC, Wang CT. 2012. Neuronal differentiation of induced pluripotent stem cells in hybrid polyester scaffolds with heparinized surface. Colloids Surf B Biointerfaces 100:9–15.

Le Douarin N, Kalcheim C. 1999. The neural crest, 2nd edition. Cambridge, NY: Cambridge University Press. pp 1–445.

Lee JH, Um S, Jang JH, Seo BM. 2012. Effects of VEGF and FGF-2 on proliferation and differentiation of human periodontal ligament stem cells. Cell Tissue Res 348:475–484.

Li X-W, Tian Y-H. 2009. Amplification and directional differentiation in vitro of human umbilical cord blood derived mesenchymal stem cells into neuron-like cells. J Clin Rehabil Tissue Eng Res 13:57–60.

Mruthyunjaya S, Manchanda R, Godbole R, Pujari R, Shiras A, Shastry P. 2010. Laminin-1 induces neurite outgrowth in human mesenchymal stem cells in serum/differentiation factors-free conditions through activation of FAK-MEK/ERK signaling pathways. Biochem Biophys Res Commun 391:43–48.

Ostrakhovitch EA, Byers JC, O'Neil KD, Semenikhin OA. 2012. Directed differentiation of embryonic P19 cells and neural stem cells into neural lineage on conducting PEDOT-PEG and ITO glass substrates. Arch Biochem Biophys 528:21–31.

Pelaez D, Huang CY, Cheung HS. 2013. Isolation of pluripotent neural crest derived stem cells from adult human tissues by connexin 43 enrichment. Stem Cells Dev Jun 10. Epub ahead of print.

Qian DX, Zhang HT, Ma X, Jiang XD, Xu R. 2010. Comparison of the efficiencies of three neural induction protocols in human adipose stromal cells. Neurochem Res 35:572–579.

Ribeiro D, Laguna Goya, R, Ravindran G, Vuono R, Parish CL, Foldi C, Piroth T, Yang S, Parmar M, Nikkhah G, Hjerling-Leffler J, Lindvall O, Barker RA, Arenas E. 2012. Efficient expansion and dopaminergic differentiation of human fetal ventral midbrain neural stem cells by midbrain morphogens. Neurobiol Dis 49C:118–127.

Seo BM, Miura M, Gronthos S, Bartold PM, Batouli S, Brahim J, Young M, Robey PG, Wang CY, Shi S. 2004. Investigation of multipotent postnatal stem cells from human periodontal ligament. Lancet 364:149–155.

Singhatanadgit W, Varodomrujiranon M. 2012. Osteogenic potency of a 3-dimensional scaffold-free bonelike sphere of periodontal ligament stem cells in vitro. Oral Surg Oral Med Oral Pathol Oral Radiol Aug 15. Epub ahead of print.

Song JS, Kim SO, Kim SH, Choi HJ, Son HK, Jung HS, Kim CS, Lee JH. 2012. In vitro and in vivo characteristics of stem cells derived from the periodontal ligament of human deciduous and permanent teeth. Tissue Eng Part A 18:2040–2051.

Wu Y, Cao H, Yang Y, Zhou Y, Gu Y, Zhao X, Zhang Y, Zhao Z, Zhang L, Yin J. 2012. Effects of vascular endothelial cells on osteogenic differentiation of noncontact co-cultured periodontal ligament stem cells under hypoxia. J Periodontal Res 48:52–65.

Zhang C, Li J, Zhang L, Zhou Y, Hou W, Quan H, Li X, Chen Y, Yu H. 2012a. Effects of mechanical vibration on proliferation and osteogenic differentiation of human periodontal ligament stem cells. Arch Oral Biol 57:1395–1407.

Zhang J, An Y, Gao LN, Zhang YJ, Jin Y, Chen FM. 2012b. The effect of aging on the pluripotential capacity and regenerative potential of human periodontal ligament stem cells. Biomaterials 33:6974–6986.

Zhou Y, Chen KS, Gao JB, Han R, Lu JJ, Peng T, Jia YJ. 2012. miR-124-1 promotes neural differentiation of rat bone marrow mesenchymal stem cells. Zhongguo Dang Dai Er Ke Za Zhi 14:215–220.